

Multiple-point source solution of the Mw7.2 Van earthquake, October 23, 2011, Eastern Turkey.

J. Zahradnik¹⁾, E. Sokos²⁾

¹⁾ Charles University in Prague, Faculty of Mathematics and Physics, Czech Republic
(e-mail: Jiri.Zahradnik@mff.cuni.cz)

²⁾ University of Patras, Department of Geology, Seismological Laboratory, Greece.
(email: esokos@upatras.gr)

Report submitted to EMSC on November 1, 2011

Abstract

This paper shows how the main asperity positions of Van earthquake are constrained by five near stations of the National Strong Motion Network of Turkey (TR-KYH), in the frequency range below 0.2 Hz. Location of the hypocenter is not solved here. Identification of multiple point sources is performed with a constant focal mechanism, determined by the DC-constrained calculation of the major subevent. Iterative deconvolution with free deviatoric mechanism would erroneously trade the source finiteness with a strong non-DC part of the major subevent. A possible spatio-temporal scenario of Van earthquake (calculated without use of the hypocenter position) consists of two or three major DC sources, following each other towards south-west, with decreasing size and increasing origin time. This is a robust result, constrained by existence of two stations in the strike and anti-strike direction (TR-KYH 5601 and 6503, respectively). The largest asperity seems to be at greater depth, but this aspect is less certain. Less certain is also a possible continuation of the rupture process towards north-east of the main subsource.

Introduction

One week after the damaging event seismological agencies have provided various hypocenter locations and centroid-moment-tensor (CMT) solutions of the mainshock. Although there is no doubt that the earthquake had a reverse mechanism, the spatial variation of the hypocenters and centroids is huge, of the order of dozens kilometers. It is therefore quite difficult to perform detailed finite-source slip inversions. The objective of this report is to find out whether near-source strong motion data from the National Strong Motion Network of Turkey (TR-KYH), freely available on Internet, might throw some light on the position and timing of main asperities, because such knowledge will be useful for subsequent source studies, as well as Coulomb stress change studies, or studies of the aftershock spatial distribution. The study also demonstrates some problems, which might be faced in quick automated assessment of the earthquake effects, such as spurious non-DC components, potentially biasing the source model.

Data and Method

We use five near stations, 001_6503, 002_1302, 003_0401, 004_4901, 005_5601, where 001 to 005 is our numbering, while the station number after underscore refers to the TR-KYH network (Fig. 1). Their epicentral distances range from 40 to 170 km, with most of them beyond 110 km. We initially invert displacement waveforms in the frequency range 0.05 to 0.10 Hz, later also 0.05 to 0.20 Hz. Green functions are calculated by the discrete wavenumber method (Bouchon, 1981, AXITRA code of Coutant, 1989) in a 1D crustal model of Novotny et al. (2001). In the distance and frequency range under study the choice of the model is not critical. The multiple-point source moment-tensor

inversion method, with ISOLA freely available Fortran code and Matlab GUI (Sokos and Zahradnik, 2008), is employed.

Table 1. Mainshock location from agencies in Turkey.

Agency	Lat °N	Lon °E	Origin time	Depth (km)
TR-KYH	38.6890	43.4657	10:41:20	19
KOERI	38.7578	43.3602	10:41:21	5

Table 2. Centroid moment tensors (DC part) by two global agencies and this study. Our preferred solution is highlighted.

Agency	strike/dip/rake (°)	strike/dip/rake (°)	Lat °N	Lon °E	Depth (km)
Global CMT	248 / 36 / 59	104 / 60 / 110	38.67	43.42	15
USGS CMT	272 / 19 / 101	80 / 71 / 86	39.451	43.354	16
Devia	220 / 75 / 77	82 / 20 / 131	38.689	43.466	15
DC-constr	236 / 46 / 70	84 / 48 / 110	38.779	43.351	15

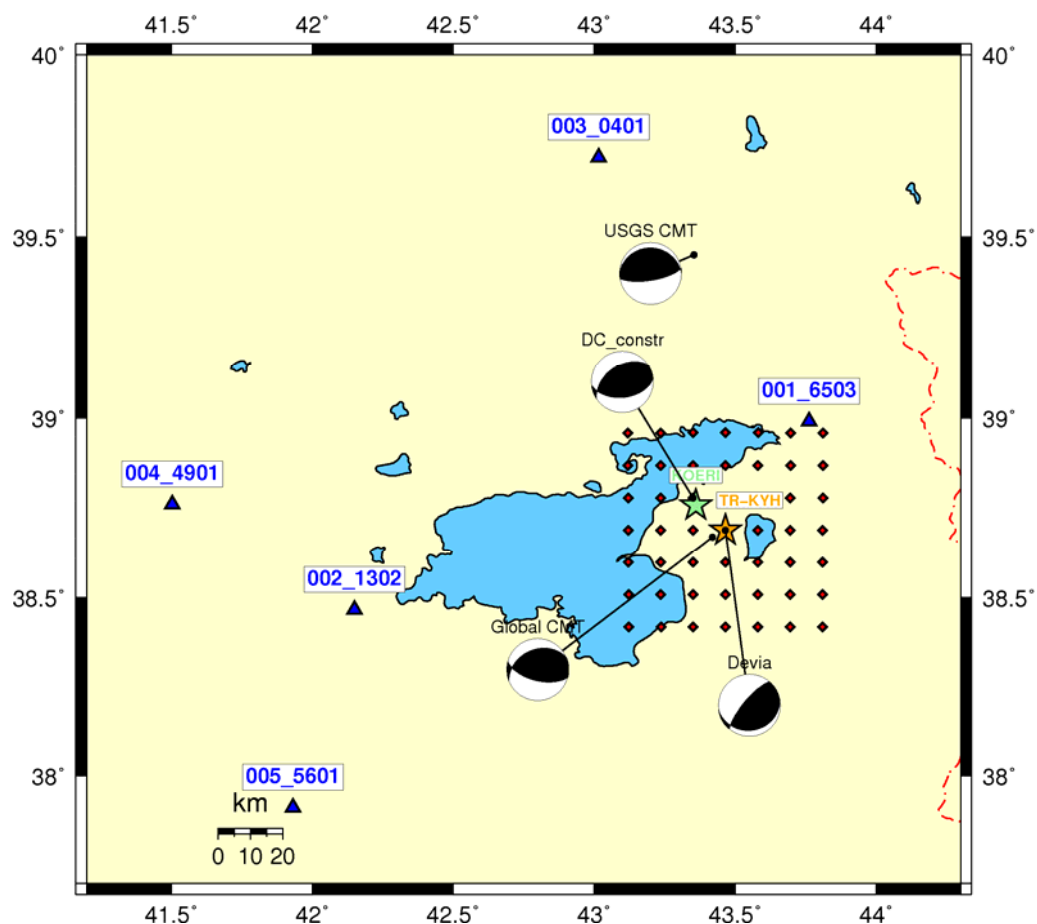


Figure 1. Five seismic stations of TR-KYH used in this paper (blue triangles), two epicenter locations of the mainshock (stars and Table 1), four focal mechanism solutions (beachballs, Table 2), and a horizontal grid of trial source positions at the depth of 15 km (red diamonds).

The moment tensors (MT) are calculated by the least-square fitting of the complete waveforms in the time domain. Possible modes of the ISOLA MT inversion include the full MT, deviatoric MT, DC-constrained MT and the inversion with fixed DC mechanism (in the latter case only the position, time and moment are calculated). No artificial temporal adjustments are performed (Zahradnik et al., 2008a). Multiple sources are calculated by the so-called iterative deconvolution (Kikuchi and Kanamori, 1991; Zahradnik et al., 2005). Quality of the solution is first estimated by the condition number, and, if the least-square problem is well posed, the overall match between observed and synthetic seismogram is quantified by the global variance reduction (VR); additionally, user can also check the VR values of the individual components. The source positions and importantly also their origin times are grid-searched. The moment-rate time function of the subsources is assumed known; we use triangles of the 10 sec duration. Naturally, at low frequencies this choice is of little effect, except importance for the correct moment values.

Note that ISOLA code does not need any information about rupture nucleation point and time. Hypocenter is merely used as a reference point (the coordinate origin). Also rupture velocity is not prescribed. Absence of these constraints is very important since the unconstrained method is much less vulnerable to inevitable inaccuracies of the mentioned parameters. This feature (absence of the constraints) makes ISOLA code particularly suitable in early stages of the investigation. See, e.g., Gallovic et al. (2009), Zahradnik and Gallovic (2010), Gallovic and Zahradnik (2011), explaining also how to proceed from simple to complex models.

Results

Experiment 1 – deviatoric (non-DC) single point-source inversion at $f < 0.1$ Hz

The first objective was to understand whether the low-frequency data ‘see’ the source as a single point, or as many subsources, and what is the position of the dominant point source (the major asperity). To this goal, forty-nine trial point-source positions were examined in a horizontal 10x10km grid (Fig. 1), centered on the TR-KYH epicenter (Table 1). The same grid of trial positions was tested at three depths, i.e. 10, 15 and 20 km, with little difference and with formally optimal results at 15km.

The single-point source inversion in the deviatoric mode preferred the central point of the grid. The global VR was 0.49, and the waveform match of station 001 was very poor. The strike, dip and rake of this solution are shown in Table 2 as “Devia”. The DC-percentage of this deviatoric solution was as low as 43%. The first subevent had moment magnitude $M_w = 6.86$. After seeking three more subevents, two of them having moment as large as $\frac{1}{2}$ of the major one, the global VR and M_w increased, the fit at station 001 improved a bit, but still it was not satisfactory. All subevents had reverse mechanism, but highly variable.

This experiment clearly demonstrated that in the frequency range under study ($f < 0.1$ Hz) the near-station data already recognize the finite-source extent and “move” this information immediately into a strong non-DC component of the first (major) subevent. Similar observations were made by Zahradnik et al. (2008b). As such, with the first subsource being already strongly biased, the deviatoric inversion of a multiple-point source has no sense. This simple rule of thumb is often overlooked in routine studies, which mostly emphasize the improvement of the waveform fit.

Experiment 2 – DC-constrained single point-source inversion at $f < 0.1$ Hz

The DC-constrained inversion (using the Lagrange multipliers) was applied to the MT grid search in the horizontal trial plane. The dominant subsource 1 moved to the neighboring grid point, 10 km to the north and 10 km to the west with respect to the grid center (TR-KYH epicenter), and it changed considerably its focal mechanism (“DC-constr” in Table 2). Mainly the dip of both nodal planes has

changed, making solution closer to the Harvard Global CMT and USGS CMT solutions. The fit of seismograms with one subsource was not good enough ($VR=0.46$), and mainly the station 001 amplitudes remained highly overestimated by the synthetics.

To validate the position of the major subevent, we also fixed the focal mechanism at the strike/dip/rake values of Global CMT and searched the position. It resulted in the same position as in our DC-constrained approach. Prescribing the source angles of USGS CMT resulted in a different position, but the waveform fit deteriorated.

This experiment well indicated that the position of the major asperity shown in Table 2 under “DC-constr” is reasonable, but it also showed that data (although only at $f < 0.1$ Hz) still require more source complexities. Station 001, the nearest station with relatively small amplitudes in the 0.05-0.10 Hz range, was detected as the most challenging to fit, and the most sensitive.

Experiment 3 – preliminary multiple point-source inversion with fixed DC mechanism in horizontal plane and $f < 0.1$ Hz

To obtain multiple point-source subevents, the focal mechanism was constrained to be constant (same for all subevents), 100% DC, with the strike/dip/rake angles equal to the values obtained in Experiment 2. Several tests, still in the horizontal grid of trial sources, proved that additional subevents improve the fit, mainly at station 001, if they are situated towards south or south-west from the main asperity (hence indication that station 001 has its small low-frequency amplitudes caused probably by its anti-directive position). To better analyze such a possibility, we had to assess the orientation of the fault plane.

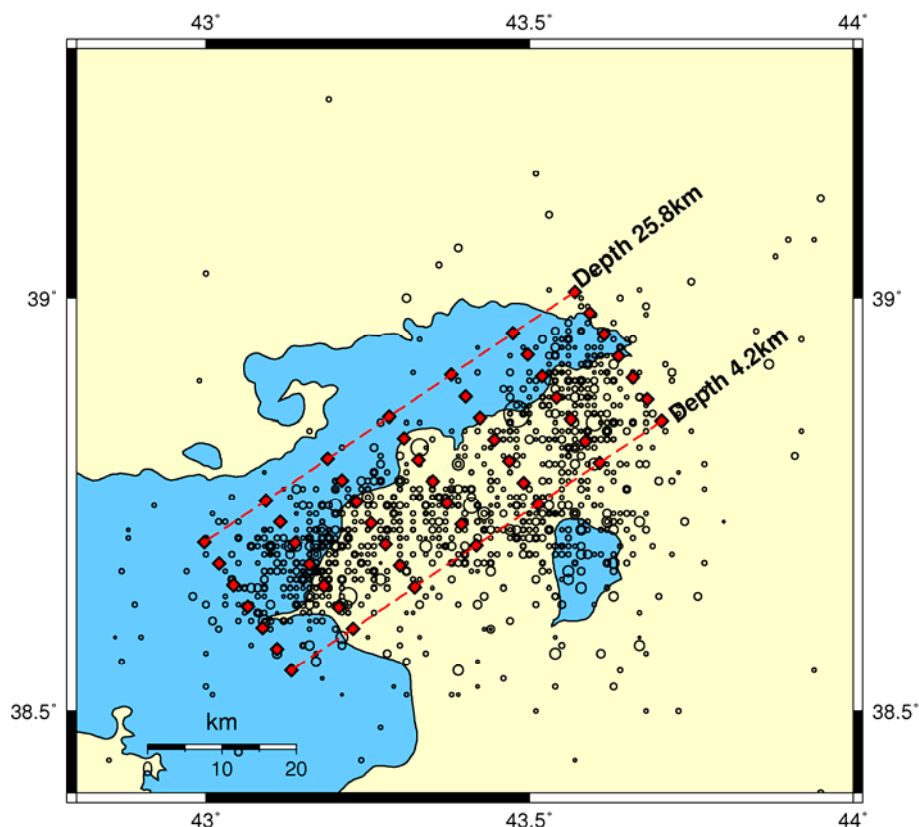


Figure 2. Distribution of aftershocks (using location data available at the EMSC web page). Superimposed is the grid of trial sources (red diamonds) used to construct the source model on the north-dipping fault plane. Bottom and top of the grid are situated at the depth of 25.8 km (the NW edge) and 4.2 km (the SE edge), respectively. The grid is centered at a point identified in this paper by means of the waveform inversion, independently of the aftershock pattern, and also independently on the mainshock hypocenter location.

Experiment 4 – the fault-plane identification

The aftershock distribution published on web pages of EMSC (to the date of writing this report, i.e. Oct. 30), see also Fig. 2, indicated a very compact and almost rectangular pattern. Its size of about 60x20 km in map view corresponds to the expected size of the Mw~7 event according to empirical relations (Somerville et al., 1999) and assuming a relatively low-angle dip, say 50°, or less. We also noticed that the strike of the pattern is almost parallel to the coast of the Van Lake, suggesting the fault strike of about 45° for a south-dipping plane, or 225° for a north-dipping plane. Comparing the Global CMT, USGS CMT and our DC-constrained solutions in Table 2, they consistently show that the only nodal plane well explaining the strike of the aftershock pattern is the north-dipping nodal plane. Another common feature of these three solutions is that their north-dipping nodal plane has a smaller dip than the other nodal plane.

Trying to support the hypothesis of the north-dipping fault plane we applied the HC method (Zahradnik et al., 2008c). From two planes passing through centroid, and having strike and dip corresponding to the CMT solution, the fault plane is that one encompassing hypocenter. Using our DC-constrained CMT solution (the position and angles of Table 2) no clear preference of any plane can be made when comparing with the hypocenters of Table 1. The only exception would be the KOERI epicenter in case that the hypocentral depth increases from the reported 5 km to 13 km; such a hypothetical hypocenter would have a smaller distance from the north-dipping plane (0.7 km) than from the south-dipping one (3.2 km). This is merely a speculation, so the relative position of the asperity and the hypocenter of Van earthquake remains to be a challenge for future studies. Anyway, we continue with the north-dipping plane indicated above by the aftershocks.

Experiment 5- multiple point-source inversion on the aftershock-suggested fault plane, fixed DC mechanism and $f < 0.2$ Hz

We adopted a grid of trial sources in the north-dipping plane (strike 236°, dip 46°), with the 10 and 5 km increments along strike and dip, respectively. We centered the grid in the position of the DC-constrained solution of Table 2, see Figs. 2 and 3. Multiple subevents were searched to optimize the global waveform fit and, at the same time, to have a reasonable agreement at the critical station 001, the nearest station of relatively low observed amplitudes (in the low-frequency range). We performed many trial-and-error calculations. The experiments included, for example, modification of the used frequency range, removal of some stations, and application of various weights. The waveform fit was almost constant, not excellent - not bad (as expected with a relatively small number of the model parameters), and we appreciated a reasonable robustness of the results. Specifically, we always obtained two major subevents, the smaller one being displaced with respect the major one towards south-west. The other (even smaller) subevents were less stable as for their position and timing. Four subevents together resulted in VR=0.65 (at $f < 0.1$ Hz) and Mw=7.1. Therefore, encouraged by this result, we increased the frequency range: 0.05 to 0.20 Hz. Still in this range we found the same behavior, hence we present an example up to 0.2 Hz. It refers to the inversion without weights.

A possible multiple point source model is shown in Fig. 3 and Table 3. The real and synthetic waveforms are compared in Fig. 4 (VR=0.51 up to 0.2 Hz and 0.65 up to 0.1 Hz). The solution is physically sound: Two major subevents follow each other towards south-west with decreasing moment, decreasing depth and increasing source time. Note the 14 km distance between them, and the corresponding ~3-sec delay. These numbers cannot be used to estimate the rupture velocity. The rupture velocity is a phenomenon within each asperity, and, as such, it is below the level of our resolution. On the other hand, the complexity of the fault process seems to be indicated well by this simple model, and it even provides a good explanation of the critical station 001. Plausibility of the model comes from the availability of the stations situated along the fault strike and anti-strike

direction (Zahradnik and Gallovic, 2010; Gallovic and Zahradnik, 2011). Even better constrained models might be found when including more stations in the anti-strike direction from Iran.

When checking robustness of the result, e.g. by removing some stations (but always keeping those in the strike and anti-strike direction), at least two major subevents always appeared, the second one (in temporal order) being shifted towards south-west; their relative depth position was less stable.

Table 3. The multiple-point source solution of this study. All subevents have a fixed DC mechanism (DC-constr of Table 2). Rupture time is expressed with respect to the origin time value of TR-KYH (Table 1). Total moment of this solution, derived for frequencies 0.05-0.20 Hz, is $4.88e19$ Nm, i.e. moment magnitude $M_w=7.1$. The most significant contributions are highlighted.

Lat °N	Lon °E	Depth (km)	Rupture time (s)	Moment (Nm)	Cumulative Moment (Nm)	Cumulative VR
38.779	43.351	15.0	6.90	2.28e19	2.29e19	0.34
38.676	43.299	7.80	9.90	1.49e19	3.78e19	0.47
38.853	43.564	11.40	7.50	.584e19	4.37e19	0.49
38.626	43.204	7.80	14.70	.517e19	4.88e19	0.51

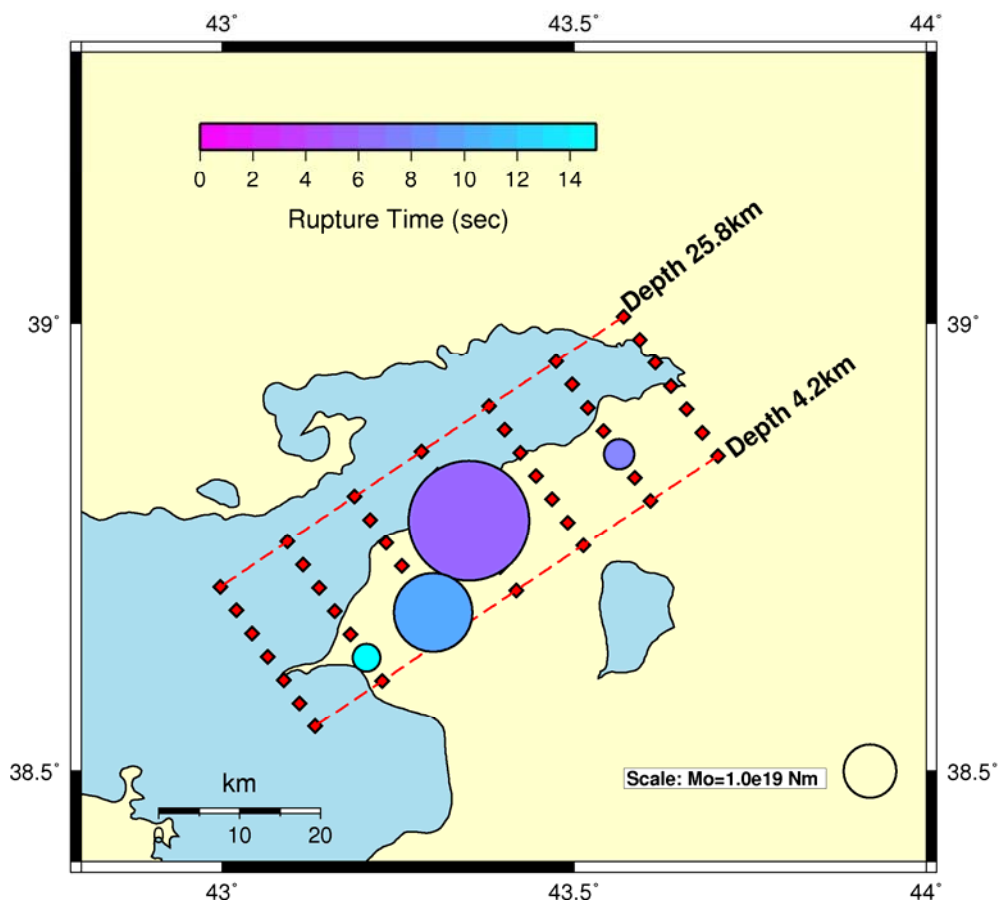


Figure 3. The grid of trial sources on the north-dipping plane (red diamonds, same as in Fig. 2), and a selected example of the multiple-point source solution of this study up to 0.2 Hz (circles and Table 3). Radius of the circles is proportional to the seismic moment, their color shows the rupture time. The solution is independent on the hypocenter position.

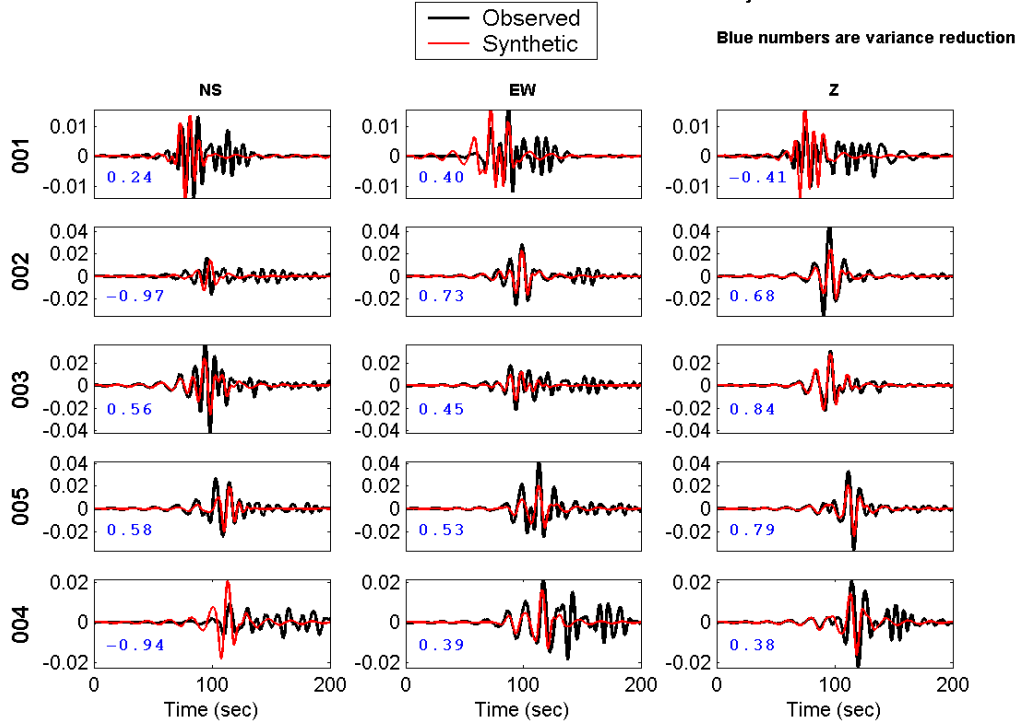


Figure 4. Comparison of the observed seismograms (black) and synthetics (red) in the frequency range 0.05–0.20 Hz. Global variance reduction is $VR=0.51$ (and 0.65 when considering $f < 0.1$ Hz). The plot corresponds to the solution of Table 3 and Fig. 3. Note the small displacement amplitudes (in meters) at station 001 in this frequency range. Just this information (the low-frequency anti-directivity effect at 001) strongly constrained the source model. On the contrary, in full frequency range, the same station 001 (6503) had the largest peak-ground acceleration among all TR-KYH stations, 0.18 g.

Conclusion

Existing reports of the hypocenter and centroid position of the Van earthquake, given by various agencies, differ of each other considerably. In order to facilitate future detailed studies, e.g. the slip inversions and/or strong motion simulations, main slip zones (asperities) must be better identified. This paper shows how the asperity positions are constrained by five near stations of the National Strong Motion Network of Turkey (TR-KYH) in the frequency range below 0.2 Hz, where limited knowledge of the specific crustal structure is not critical. In particular, the nearest station (6503 according to TR-KYH, i.e. 001 in this paper) provided a strong control on the source model, being most likely the anti-directive station. The term anti-directive is used with respect to an integral effect of the whole finite source, not excluding possibility that some of the individual asperities ruptured radially, or even in a direction towards station 001. Rupture propagation within the individual asperities was not analysed. The paper focused on identification on multiple point sources with fixed focal mechanism. Fixing the 100% DC mechanism is particularly important since the iterative deconvolution with free deviatoric mechanisms would erroneously trade the source finiteness with a strong spurious non-DC part of the major subevent, mainly because of the fault-to-stations proximity. A possible spatio-temporal scenario of Van earthquake consists of two or three major subevents, following each other towards south-west, with decreasing size and increasing origin time. The solution is fully independent of the (so-far unsure) location of the hypocenter.

Acknowledgement

The authors thank to National Strong Motion Network of Turkey (TR-KYH) for free Internet access of accelerograms. Discussions with Frantisek Gallovic and his helpful comments to this manuscript are highly appreciated. The work was financially supported by the following grants in the Czech Republic: GACR 210/11/0854 and MSM 0021620860.

References

- Bouchon, M. (1981). A simple method to calculate Green's functions for elastic layered media, *Bull. Seism. Soc. Am.* 71, 959-971.
- Coutant, O., 1989. Programme de simulation numerique AXITRA. Res. Report LGIT, Grenoble.
- Gallovic, F., J. Zahradnik, D. Krizova, V. Plicka, E. Sokos, A. Serpetsidaki, and G.-A. Tselentis (2009). From earthquake centroid to spatial-temporal rupture evolution: Mw6.3 Movri Mountain earthquake, June 8, 2008, Greece, *Geophys. Res. Lett.*, 36, L21310.
- Gallovic, F., and J. Zahradnik, J. (2011). Toward understanding slip-inversion uncertainty and artifacts II: singular value analysis, *J. Geophys. Res.*, 116, B02309.
- Kikuchi, M., and H. Kanamori (1991). Inversion of complex body waves. III, *Bull. Seism. Soc. Am.* 81, 2335–2350.
- Novotny, O., J. Zahradnik, and G.-A. Tselentis (2001). North-western Turkey earthquakes and the crustal structure inferred from surface waves observed in the Corinth Gulf, Greece, *Bull. Seism. Soc. Am.* 91, 875–879.
- Sokos, E., and J. Zahradnik (2008). ISOLA A Fortran code and a Matlab GUI to perform multiple-point source inversion of seismic data, *Computers & Geosciences* 34, 967-977.
- Somerville, P., K. Irikura, R. Graves, S. Sawada, D. Wald, N. Abrahamson, Y. Iwasaki, T. Kagawa, N. Smith, and A. Kowada (1999). Characterizing crustal earthquake slip models for the prediction of strong ground motion, *Seism. Res. Lett.* 70, 59–80.
- Zahradnik, J., Serpetsidaki, A., Sokos, E, and Tselentis, G-A. (2005). Iterative deconvolution of regional waveforms and a double-event interpretation of the 2003 Lefkada earthquake, Greece, *Bull. Seism. Soc. Am.* 95, 159-172.
- Zahradnik, J., J. Jansky, and V. Plicka (2008a). Detailed waveform inversion for moment tensors of M~4 events: Examples from the Corinth Gulf, Greece, *Bull. Seism. Soc. Am.* 98, 2756–2771.
- Zahradnik, J., E. Sokos, G.-A. Tselentis, and N. Martakis (2008b). Non-double-couple mechanism of moderate earthquakes near Zakynthos, Greece, April 2006; explanation in terms of complexity, *Geophysical Prospecting* 56, 341–356.
- Zahradnik, J., F. Gallovic, E. Sokos, A. Serpetsidaki, and G.A. Tselentis (2008c). Quick fault-plane identification by a geometrical method: application to the Mw6.2 Leonidio earthquake, January 6, 2008, Greece, *Seismol. Res. Lett.* 79, 653–662.
- Zahradnik, J., and F. Gallovic (2010). Toward understanding slip-inversion uncertainty and artifacts, *J. Geophys. Res.*, 115, B09310.